International Journal of Heat and Mass Transfer 52 (2009) 337–344

Contents lists available at ScienceDirect

International Journal of Heat and Mass Transfer

journal homepage: www.elsevier.com/locate/ijhmt

The onset of convection in a porous layer induced by viscous dissipation: A linear stability analysis

A. Barletta [a,*], M. Celli [a], D.A.S. Rees [b,1]

[a] Dipartimento di Ingegneria Energetica, Nucleare e del Controllo Ambientale (DIENCA), Laboratorio di Montecuccolino, Facoltà di Ingegneria, Università di Bologna, Via dei Colli 16, I–40136 Bologna, Italy
[b] Department of Mechanical Engineering, University of Bath, Bath, BA2 7AY, UK

ARTICLE INFO

Article history:
Received 14 September 2007
Received in revised form 27 May 2008
Available online 31 July 2008

Keywords:
Laminar flow
Mixed convection
Darcy model
Porous medium
Linear Stability
Viscous dissipation

ABSTRACT

The effect of viscous dissipation on parallel Darcy flow in a horizontal porous layer with an adiabatic lower boundary and an isothermal upper boundary is discussed. The presence of viscous dissipation serves to cause a nonlinear temperature profile within the layer. The linear stability of this nonisothermal base flow is then investigated with respect to the onset of convective rolls. The solution of the linear equations for the perturbation waves is determined analytically by a power series method, and the results are confirmed using a direct numerical approach using a fourth order Runge Kutta method. The neutral stability curve and the critical value of the governing parameter $R = Ge\,Pe^2$ are obtained, where Ge is the Gebhart number and Pe is the Péclet number. The effect of an imperfect isothermal boundary condition at the upper boundary is investigated by considering finite values of the Biot number.

1. Introduction

The onset of convection in a horizontal fluid-saturated porous layer heated from below has been widely studied in the last few decades. The interest in this subject is related both to geophysical research and to engineering design. Possible applications include the analysis of water currents in a porous rock, the underground spread of pollutants, the enhancement of the performance in building insulation, solar energy collectors and solar ponds. Wide and detailed discussions of the literature on this subject can be found in the book by Nield and Bejan [1] and the reviews of Rees [2] and Tyvand [3].

The early papers of Horton and Rogers [4] and Lapwood [5] presented the first linearised stability analyses of what has become known widely as either the Horton–Rogers–Lapwood (HRL) problem or the Darcy–Bénard (DB) problem. The former links us to the pioneers of stability theory in porous media, while the latter emphasizes the strong link with the Rayleigh-Bénard problem. The classical DB problem consists of a basic motionless state with a uniform temperature drop across the layer with warmer fluid lying below cooler fluid.

Very many authors have developed variants of this basic stability problem either by employing porous models that are more complicated than Darcy's law, or by altering the external conditions, such as imperfectly conducting boundaries or the presence of internal heating, rotation or vertical throughflow. Of most interest here is the study of Prats [6] who investigated the effect of a uniform parallel basic flow in the layer which might be caused by applying a uniform horizontal pressure along the layer. By using a moving frame of reference Prats proved that this uniform basic flow does not alter the condition for the onset of instability. In Prats' treatment, the critical value of Rayleigh number, Ra_{cr}, is the same as in the DB problem, viz. $4\pi^2$. Moreover, the full nonlinear equations, when written in the moving frame, reduce to those which apply when there is no basic flow. Therefore, the full nonlinear behaviour of the DB problem is recovered in an infinitely long layer. One other consequence is that there is no preferred direction for the roll orientation at onset, a property which it does not share with Bénard–Poiseuille convection.

With regard to what we shall call the Darcy–Bénard–Prats (DBP) problem, there exist some recent papers which have extended the work of Prats [6]. Rees [7] considered the effect of quadratic form drag in the momentum equation. He showed that the critical Darcy–Rayleigh number, Ra_{cr}, depends on both the form drag coefficient and on the base flow velocity. Moreover, the critical Darcy–Rayleigh number is also dependent on the roll orientation, with longitudinal rolls forming the preferred pattern. The additional effects of lateral confinement were considered by

* Corresponding author.
E-mail addresses: antonio.barletta@mail.ing.unibo.it (A. Barletta), michele.celli@mail.ing.unibo.it (M. Celli), D.A.S.Rees@bath.ac.uk (D.A.S. Rees).
[1] Present address: Department of Mathematics, University of Bristol, Bristol BS8 1TW, UK.

0017-9310/$ - see front matter © 2008 Elsevier Ltd. All rights reserved.
doi:10.1016/j.ijheatmasstransfer.2008.06.001

Nomenclature

a	nondimensional wave number, Eq. (28)
A_n	nth series coefficient, Eq. (36)
Bi	Biot number, hL/k
c_p	specific heat at constant pressure
c_{wave}	nondimensional phase velocity, Eq. (35)
g	modulus of gravitational acceleration
$\mathbf{g}$	gravitational acceleration
G	nondimensional parameter, $Ge(\cos\chi)^2$
Ge	Gebhart number, Eq. (13)
h	external heat transfer coefficient
K	permeability
k	thermal conductivity
L	channel height
$\mathscr{L}_n$	differential operator, Eqs. (A11), (A12)
n	integer number
P	nondimensional parameter, $Pe/\cos\chi$
Pe	Péclet number, Eq. (16)
R	nondimensional parameter, $GePe^2$
$\Re$	real part
$\mathbf{s}$	unit vector parallel to the base flow direction
t	nondimensional time, Eq. (7)
T	nondimensional temperature, Eq. (7)
T_w	upper boundary temperature or external temperature
u, v, w	nondimensional velocity components, Eq. (7)
U, V, W	nondimensional velocity disturbances, Eq. (17)
$\bar{\mathbf{u}}_B$	base flow velocity
x, y, z	nondimensional coordinates, Eq. (7)

Greek symbols

α	thermal diffusivity
β	volumetric coefficient of thermal expansion
γ	reduced exponential coefficient, Eq. (29)
ϵ	nondimensional parameter, Eq. (A3)
θ	nondimensional temperature disturbance, Eq. (17)
$\Theta(y)$	nondimensional function, Eq. (28)
λ	exponential coefficient, Eq. (28)
λ_1, λ_2	real and imaginary parts of λ
ν	kinematic viscosity
ρ	mass density
σ	heat capacity ratio
χ	angle between base flow direction and x-axis
ψ	nondimensional streamfunction, Eq. (24)
$\Psi(y)$	nondimensional function, Eq. (28)

Superscript, subscripts

–	dimensional quantity
B	base flow
cr	critical value

Delache, Ouarzazi and Néel [8]; these authors found discontinuous transitions between preferred roll states. Postelnicu [9] extended the work of Rees [7] by combining it with the work of Banu and Rees [10], who employed the two-temperature model for heat conduction. This model involves an inter-phase heat transfer coefficient to account for the absence of local thermal equilibrium between the solid and fluid phases. A comprehensive set of results is presented by Postelnicu [9] showing the detailed effect on the critical Darcy–Rayleigh number and wavenumber of the inertia parameter, the flow rate and the three parameters that are associated with local thermal nonequilibrium.

The aim of the present paper is to consider the following variant on the DBP problem. In the above-cited works thermoconvective instability was driven by an unstable temperature gradient that is imposed externally. In the present paper we shall assume that there is no imposed temperature gradient across the layer, but rather that heat is generated internally by the action of viscous dissipation. In particular the upper surface will be taken to be isothermal (infinite-Biot number), while the lower surface is thermally insulated. The former boundary condition is relaxed later in the paper by using a finite-Biot-number condition to represent external heat transfer to the ambient temperature.

A linear stability analysis of oblique rolls which are orientated arbitarily with respect to the uniform base flow direction is performed. The disturbance equations are solved both analytically by a series method and numerically by a fourth order Runge Kutta method. We present information on how the critical Darcy–Rayleigh number and wavenumber vary with the Gebhart and Péclet numbers. Asymptotic expressions for the critical quantities vs the Péclet number are obtained.

2. Mathematical model

We shall consider laminar buoyant flow in a horizontal parallel channel with height L (see Fig. 1). Both the Darcy model and the Boussinesq approximation are invoked. The components of seepage velocity along the $\bar{x}$-, $\bar{y}$- and $\bar{z}$-directions are denoted by $\bar{u}$, $\bar{v}$ and $\bar{w}$, respectively. The lower boundary wall $\bar{y} = 0$ is assumed to be adiabatic, while the upper boundary wall $\bar{y} = L$ is supposed to be isothermal with temperature T_w. Both boundary walls are impermeable. Later in the paper we relax the assumption of having a perfectly conducting upper boundary.

The governing mass, momentum and energy balance equations can be expressed as

$$\frac{\partial \bar{u}}{\partial \bar{x}} + \frac{\partial \bar{v}}{\partial \bar{y}} + \frac{\partial \bar{w}}{\partial \bar{z}} = 0, \tag{1}$$

$$\frac{\partial \bar{v}}{\partial \bar{x}} - \frac{\partial \bar{u}}{\partial \bar{y}} = \frac{g\beta K}{\nu}\frac{\partial \overline{T}}{\partial \bar{x}}, \tag{2}$$

$$\frac{\partial \bar{v}}{\partial \bar{z}} - \frac{\partial \bar{w}}{\partial \bar{y}} = \frac{g\beta K}{\nu}\frac{\partial \overline{T}}{\partial \bar{z}}, \tag{3}$$

$$\frac{\partial \bar{u}}{\partial \bar{z}} - \frac{\partial \bar{w}}{\partial \bar{x}} = 0, \tag{4}$$

$$\sigma\frac{\partial \overline{T}}{\partial \bar{t}} + \bar{u}\frac{\partial \overline{T}}{\partial \bar{x}} + \bar{v}\frac{\partial \overline{T}}{\partial \bar{y}} + \bar{w}\frac{\partial \overline{T}}{\partial \bar{z}} = \alpha\left(\frac{\partial^2 \overline{T}}{\partial \bar{x}^2} + \frac{\partial^2 \overline{T}}{\partial \bar{y}^2} + \frac{\partial^2 \overline{T}}{\partial \bar{z}^2}\right) + \frac{\nu}{Kc_p}\left(\bar{u}^2 + \bar{v}^2 + \bar{w}^2\right), \tag{5}$$

where σ is the ratio between the average volumetric heat capacity $(\rho c_p)_m$ of the porous medium and the volumetric heat capacity $(\rho c_p)_f$ of the fluid. Eq. (2) has been obtained by combining the $\bar{x}$-component and the $\bar{y}$-component of Darcy's law in order to remove the explicit dependence on the pressure field; Eqs. (3) and (4) were obtained in a similar manner.

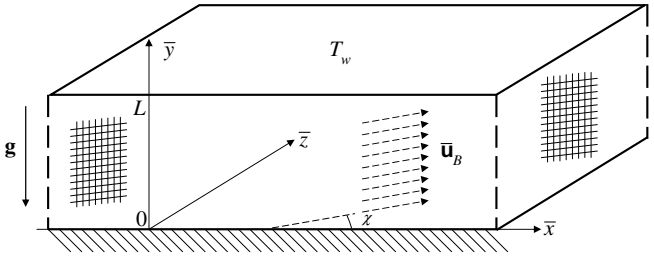

Fig. 1. Sketch of the horizontal porous channel.

The velocity and temperature boundary conditions are expressed as

$$\bar{y}=0: \quad \bar{v}=0=\frac{\partial \overline{T}}{\partial \bar{y}}, \qquad \bar{y}=L: \quad \bar{v}=0, \quad \overline{T}=T_w. \tag{6}$$

In this paper, a horizontal pressure gradient is applied that produces a uniform flow of magnitude $\bar{u}_B$ at an angle χ to the x-direction; this is defined more precisely below.

2.1. Nondimensionalization

Let us introduce dimensionless variables such that

$$(\bar{x},\bar{y},\bar{z})=(x,y,z)L, \quad \bar{t}=t\,\frac{\sigma L^2}{\alpha}, \quad (\bar{u},\bar{v},\bar{w})=(u,v,w)\,\frac{\alpha}{L},$$
$$\overline{T}=T_w+T\,\frac{v\alpha}{K c_p}. \tag{7}$$

Then, Eqs. (1)–(5) can be rewritten as

$$\frac{\partial u}{\partial x}+\frac{\partial v}{\partial y}+\frac{\partial w}{\partial z}=0, \tag{8}$$
$$\frac{\partial v}{\partial x}-\frac{\partial u}{\partial y}=Ge\,\frac{\partial T}{\partial x}, \tag{9}$$
$$\frac{\partial v}{\partial z}-\frac{\partial w}{\partial y}=Ge\,\frac{\partial T}{\partial z}, \tag{10}$$
$$\frac{\partial u}{\partial z}-\frac{\partial w}{\partial x}=0, \tag{11}$$
$$\frac{\partial T}{\partial t}+u\,\frac{\partial T}{\partial x}+v\,\frac{\partial T}{\partial y}+w\,\frac{\partial T}{\partial z}=\frac{\partial^2 T}{\partial x^2}+\frac{\partial^2 T}{\partial y^2}+\frac{\partial^2 T}{\partial z^2}+u^2+v^2+w^2, \tag{12}$$

where the Gebhart number is given by

$$Ge=\frac{g\beta L}{c_p}. \tag{13}$$

The boundary conditions (6) may be expressed in dimensionless form as

$$y=0: \qquad v=\frac{\partial T}{\partial y}=0, \qquad y=1: \qquad v=T=0. \tag{14}$$

It must be pointed out that, in most practical cases, the Gebhart number is very small. The condition $Ge=1$ is far beyond any conceivable application, as it is illustrated in Table 1 with reference to some liquids and gases. As it is shown by the last column of Table 1, the thickness L corresponding to the condition $Ge=1$, i.e., the ratio $c_p/(g\beta)$, is several kilometers. Cases with $Ge\sim O(1)$ will be considered in the following treatment just for comparison with the asymptotic case $Ge\to 0$.

2.2. Base flow

We are under the assumptions of a horizontal steady parallel flow in the direction of the unit vector $\mathbf{s}=(\cos\chi,0,\sin\chi)$ lying in the x–z-plane and of a purely vertical heat flux.

Table 1
Determination of $Ge=g\beta L/c_p$ for some typical fluids (data from Ref. [11])

Fluid	β [K^{-1}]	c_p [J kg^{-1} K^{-1}]	$g\beta/c_p$ [m^{-1}]	$c_p/(g\beta)$ [km]
Water (saturated) at 20 °C	1.8×10^{-4}	4181.8	4.2×10^{-7}	2370
Unused engine oil (saturated) at 20 °C	7×10^{-4}	1880.0	3.7×10^{-6}	274
Dry air at 300 K (atmospheric pressure)	1/300	1005.7	3.3×10^{-5}	31
Carbon dioxide at 300 K (atmospheric pressure)	1/300	871.0	3.8×10^{-5}	27

The basic state, which we shall analyse for stability, is given by,

$$u_B=Pe\cos\chi, \quad v_B=0, \quad w_B=Pe\sin\chi, \quad T_B=\frac{Pe^2}{2}(1-y^2), \tag{15}$$

where

$$Pe=\frac{\bar{\mathbf{u}}_B\cdot\mathbf{s}L}{\alpha}, \tag{16}$$

defines the Péclet number based on the uniform base flow velocity $\bar{\mathbf{u}}_B\cdot\mathbf{s}$. Obviously, it is not restrictive to assume that $\bar{\mathbf{u}}_B\cdot\mathbf{s}>0$, *i.e.* $Pe>0$.

2.3. Linearization

Perturbations of the base state given by Eq. (15) are defined as

$$u=u_B+U, \quad v=v_B+V, \quad w=w_B+W, \quad T=T_B+\theta. \tag{17}$$

On substituting Eq. (17) in Eqs. (8)–(12) and neglecting nonlinear terms in the perturbations, we obtain the linearised stability equations,

$$\frac{\partial U}{\partial x}+\frac{\partial V}{\partial y}+\frac{\partial W}{\partial z}=0, \tag{18}$$
$$\frac{\partial V}{\partial x}-\frac{\partial U}{\partial y}=Ge\,\frac{\partial \theta}{\partial x}, \tag{19}$$
$$\frac{\partial V}{\partial z}-\frac{\partial W}{\partial y}=Ge\,\frac{\partial \theta}{\partial z}, \tag{20}$$
$$\frac{\partial U}{\partial z}-\frac{\partial W}{\partial x}=0, \tag{21}$$
$$\frac{\partial \theta}{\partial t}+Pe\cos\chi\,\frac{\partial \theta}{\partial x}+Pe\sin\chi\,\frac{\partial \theta}{\partial z}-Pe^2 Vy$$
$$=\frac{\partial^2\theta}{\partial x^2}+\frac{\partial^2\theta}{\partial y^2}+\frac{\partial^2\theta}{\partial z^2}+2\,Pe\cos\chi\,U+2\,Pe\sin\chi\,W, \tag{22}$$

where use has been made of Eq. (15). The linearity of Eqs. (18)–(22) implies that, due to the superposition property, one may treat rolls of different orientations separately with regard to instability. An advantage is that each of these cases can be dealt with using a purely 2D treatment.

3. Instability with respect to rolls

We shall be introducing periodic roll solutions as the disturbance. Given that χ is an arbitrary direction it is not restrictive to consider rolls with axes along the z-direction by first setting

$$U=U(x,y,t), \quad V=V(x,y,t), \quad W=0, \quad \theta=\theta(x,y,t). \tag{23}$$

On introducing a streamfunction, ψ, such that

$$U=Pe^{-2}\,\frac{\partial\psi}{\partial y}, \quad V=-Pe^{-2}\,\frac{\partial\psi}{\partial x}, \tag{24}$$

then Eqs. (18), (20) and (21) are satisfied identically, while Eqs. (19) and (22) may be rewritten in the form

$$\frac{\partial^2\psi}{\partial x^2}+\frac{\partial^2\psi}{\partial y^2}+GePe^2\,\frac{\partial\theta}{\partial x}=0, \tag{25}$$
$$\frac{\partial\theta}{\partial t}+Pe\cos\chi\,\frac{\partial\theta}{\partial x}+y\frac{\partial\psi}{\partial x}=\frac{\partial^2\theta}{\partial x^2}+\frac{\partial^2\theta}{\partial y^2}+2\,Pe^{-1}\cos\chi\,\frac{\partial\psi}{\partial y}. \tag{26}$$

The boundary conditions fulfilled by ψ and θ are easily inferred from Eqs. (14), (15), (17) and (24), namely

$$y=0: \quad \psi=\frac{\partial\theta}{\partial y}=0, \qquad y=1: \quad \psi=\theta=0. \tag{27}$$

Solutions of Eqs. (25)–(27) are sought in the form of plane waves,

$$\psi(x,y,t) = \Re\{\Psi(y)\, e^{\lambda t} e^{iax}\}, \quad \theta(x,y,t) = \Re\{\Theta(y)\, e^{\lambda t} e^{iax}\}, \tag{28}$$

where the positive real constant a is the prescribed wave number, while $\lambda = \lambda_1 + i\lambda_2$ is a complex exponential growth rate to be determined. We shall set $\lambda_1 = 0$ in order to investigate neutral stability. Moreover, for numerical convenience we shall also set

$$\gamma = \lambda_2 + aPe\cos\chi. \tag{29}$$

By substituting Eq. (28) in Eqs. (25) and (26), we obtain

$$\Psi'' - a^2\Psi + iaR\Theta = 0, \tag{30}$$

$$\Theta'' - (i\gamma + a^2)\Theta + 2P^{-1}\Psi' - iay\Psi = 0, \tag{31}$$

where primes denote differentiation with respect to y, and where we have introduced the nondimensional parameters,

$$R = GePe^2, \qquad P = Pe/\cos\chi. \tag{32}$$

In Eq. (30) R plays the role of a Darcy–Rayleigh number as it multiplies the buoyancy term, while P is a modified Péclet number. Elimination of Θ between Eqs. (30) and (31) yields a fourth order ordinary differential equation for $\Psi(y)$, namely

$$\Psi'''' - (2a^2 + i\gamma)\Psi'' - 2iaRP^{-1}\Psi' + a^2(a^2 - Ry + i\gamma)\Psi = 0. \tag{33}$$

The boundary conditions fulfilled by $\Psi(y)$ are easily deduced from Eqs. (27), (28),

$$y = 0: \quad \Psi = \Psi''' - a^2\Psi' = 0, \qquad y = 1: \quad \Psi = \Psi'' = 0. \tag{34}$$

Eqs. (28) and (29) imply that the perturbation wave travels in the x-direction with a dimensionless phase velocity

$$c_{\mathrm{wave}} = Pe\cos\chi - \frac{\gamma}{a}. \tag{35}$$

If $c_{\mathrm{wave}} > 0$, the wave travels in the same direction of the base flow. On the other hand, if $c_{\mathrm{wave}} < 0$, the wave travels in the direction opposite to the base flow, which is unphysical.

3.1. The eigenvalue problem

The homogeneity of Eqs. (33) and (34) implies that $\Psi(y)$ is defined only up to an arbitrary overall scale factor, which means that we may set $\Psi'(0) = 1$ as a normalisation condition.

These equations form an ordinary differential eigenvalue problem for R and γ for any chosen wavenumber, a, and modified Péclet number, P. Given the definition of R in Eq. (32), this means that the critical Gebhart number may be found in terms of the Péclet number. It is more satisfying from a physical point of view to obtain a critical Péclet number as a function of the Gebhart number, but although one may plot the variation of the critical Gebhart number with Péclet number, it turns out that R remains of $O(1)$ through the physically acceptable range of values of Ge.

3.2. Series solution of the initial value problem

Eqs. (33) subject to (34) may be solved by a power series method using

$$\Psi(y) = \sum_{n=0}^{\infty} \frac{A_n}{n!}\, y^n. \tag{36}$$

The three known (complex) initial conditions are,

$$A_0 = 0, \quad A_1 = 1, \quad A_3 = a^2, \tag{37}$$

while A_2 will need to be obtained by prescribing the boundary conditions at $y = 1$, Eq. (34). Higher order coefficients A_n may be determined by substituting Eq. (36) into Eq. (33) and collecting like powers of y. One thus obtains

$$A_4 = (2a^2 + i\gamma)A_2 + 2iaRP^{-1}, \tag{38}$$

and the recursion relation

$$A_{n+4} = (2a^2 + i\gamma)A_{n+2} + 2iaRP^{-1}A_{n+1} - a^2(a^2 + i\gamma)A_n + na^2RA_{n-1}, \quad \forall\, n \geqslant 1. \tag{39}$$

The series solution given by Eq. (36) has a very rapid convergence. The real values of R and γ and the complex value of A_2 are obtained by ensuring that the two complex boundary conditions at $y = 1$ are satisfied. In all the following cases six digits of accuracy may be achieved by truncating the sum to the first 40 terms. Neutral curves may be traced out by varying the value of a, and the value which minimises R is termed the critical wavenumber, and denoted by a_{cr}.

We also used a 4th order Runge Kutta code with the shooting method as an alternative numerical procedure. In the following, all the numerical results are obtained by both methods in order to ensure their cross-validation.

3.3. Stability analysis

In the first instance, it is important to note that $P^{-1} = 0$ when considering longitudinal rolls, for which $\chi = \pi/2$. In these cases, Eq. (33) loses the RP^{-1} term, and it is possible to show that the resulting eigenvalue problem admits real eigensolutions with $\gamma = 0$. Thus the complex 4th order system reduces to a real 4th order system. The neutral stability curve for this case is given in Fig. 2, which shows that it has the classical shape for Bénard-like problems. In this case we find that

$$R_{\mathrm{cr}} = 61.8666 \qquad \text{and} \qquad a_{\mathrm{cr}} = 2.44827. \tag{40}$$

Therefore, we may state that

$$Pe_{\mathrm{cr}} = 7.8655\, Ge^{-1/2}, \tag{41}$$

where all decimal places quoted are correct. Given that, for most convection problems involving liquids, Ge can hardly be greater than 10^{-6}, unless $L \approx 1\,\mathrm{m}$ or higher, this means that we must have a relatively high flow rate within the porous layer to generate sufficient heat to cause a thermoconvective instability.

Indeed, when Ge takes extremely small values, Eq. (41) implies that Pe must be extremely large. Therefore, Eq. (33) also suggests that the RP^{-1} term is negligible in these circumstances and therefore the onset criterion is independent of χ, as in DBP problem of Prats [6].

For roll orientations other than longitudinal, the definition of P given in Eq. (32) shows that stability criteria for all roll orientations may be given in terms of the transverse roll, for which $\chi = 0$.

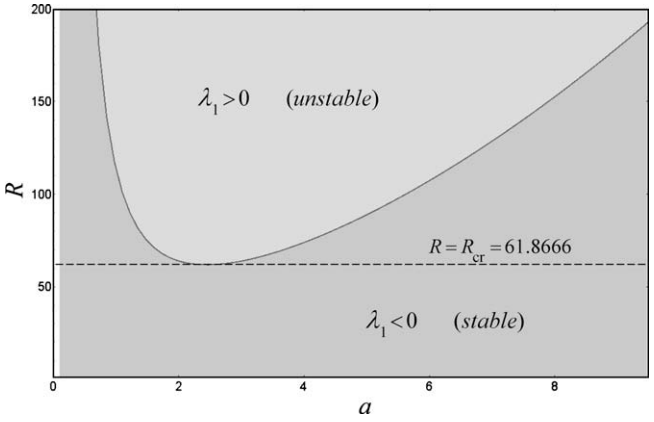

Fig. 2. Perfectly isothermal upper wall ($Bi \to \infty$): stability diagram (a, R).

In Figs. 3 and 4, we show the respective variation of R_{cr} with P and with $G = Ge\cos^2\chi$. From Eq. (32), the latter parameter is such that $R = GP^2$. Also shown are the three-term large-P asymptotic solutions given by Eq. (A35). These figures show that there is only a fairly weak variation in the critical values with both these parameters. In fact, the three-term asymptotic expansion of R_{cr} yields extremely accurate solutions over a range of G which is much bigger than is physically achievable for a porous medium. A detailed comparison between the asymptotic and the numerical data shows that the error in R_{cr} exceeds 1% once $Ge > 0.45$ or, equivalently, $Pe < 0.64$.

Fig. 5 shows how the critical wavenumber varies with G. At large values of P (or, equivalently, small values of G), the critical wavenumber is approximately constant, reducing strongly as P and G tend towards $O(1)$ magnitudes. Fig. 6 shows the reduced wavespeed, γ. In all cases the reduced wavespeed, γ, is positive, which means that the overall wavespeed, λ_2, is reduced from the speed of the base flow. Therefore rolls travel more slowly than the base flow. The variation of γ is roughly linear with P^{-1}, as shown in the Appendix. In both cases, the asymptotic expansions given in the Appendix yield extremely accurate representations of the numerical results. Finally, we note that, since $Ge \ll 1$ implies that $Pe_{cr} \gg 1$, it is highly likely that inertia/form drag effects will be significant; we intend to report on this aspect in the near future.

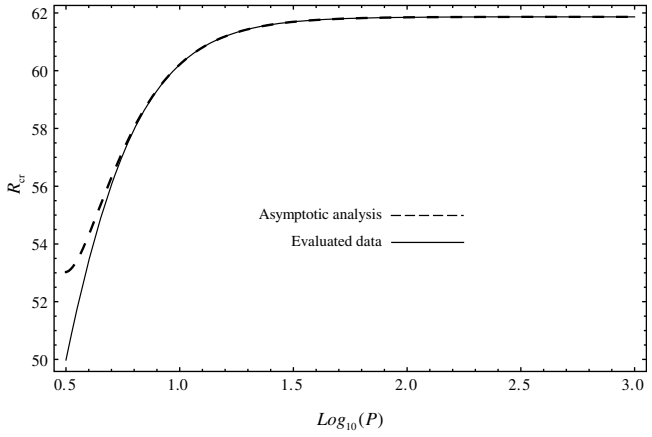

Fig. 3. Perfectly isothermal upper wall ($Bi \to \infty$). R_{cr} vs P diagram: comparison between the evaluated data and the asymptotic expansions.

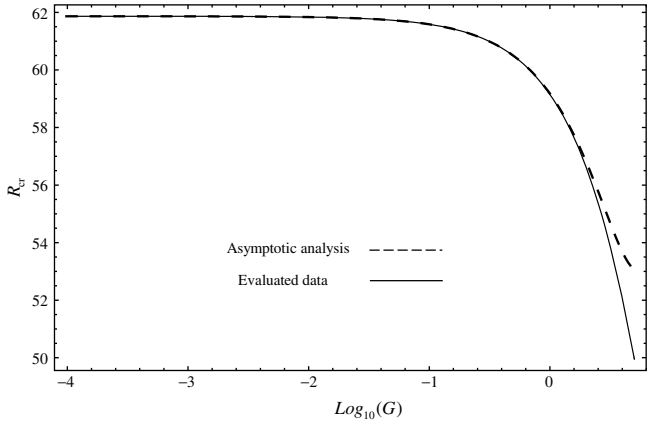

Fig. 4. Perfectly isothermal upper wall ($Bi \to \infty$). R_{cr} vs G diagram: comparison between the evaluated data and the asymptotic expansions.

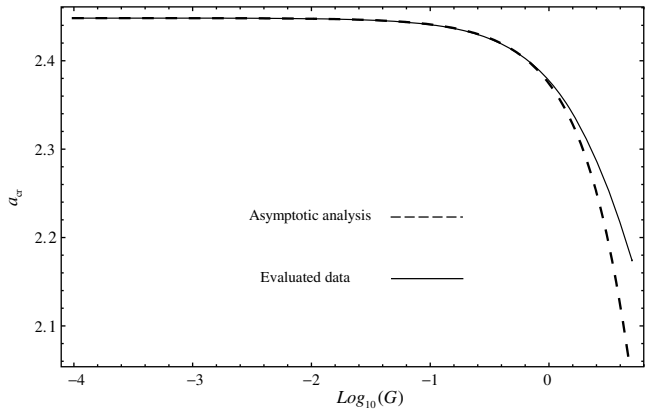

Fig. 5. Perfectly isothermal upper wall ($Bi \to \infty$). a_{cr} vs G diagram: comparison between the evaluated data and the asymptotic expansions.

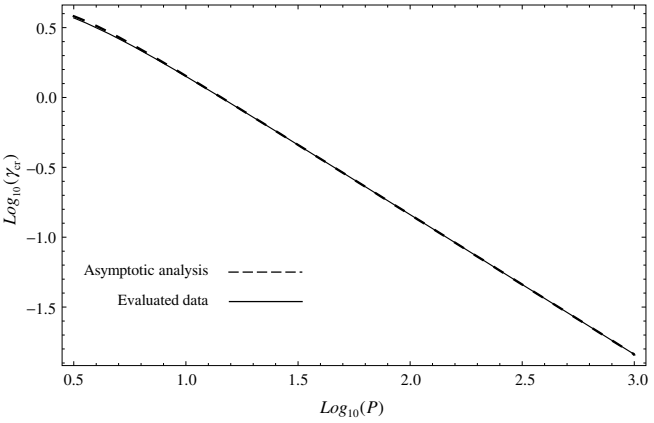

Fig. 6. Perfectly isothermal upper wall ($Bi \to \infty$). γ_{cr} vs P diagram: comparison between the evaluated data and the asymptotic expansions.

3.4. The effect of an imperfectly isothermal upper boundary wall

The practical possibility of having a perfect isothermal boundary is limited by the finite, although very high, efficiency of the thermal contact between the surface and the external environment through a properly designed convection process. Thus, a more realistic thermal condition at the upper boundary $\bar{y} = L$ is given by a third kind or Robin boundary condition. In this case, the $\bar{y} = L$ boundary condition in Eq. (6) is replaced by

$$\bar{y} = L: \quad \bar{v} = 0, \quad -k\frac{\partial \overline{T}}{\partial \bar{y}} = h(\overline{T} - T_w), \tag{42}$$

where k is the thermal conductivity and h the external heat transfer coefficient.

Then, instead of Eq. (14b), one has

$$y = 1: \quad v = 0 = \frac{\partial T}{\partial y} + Bi\,T, \tag{43}$$

where $Bi = hL/k$ is the Biot number. The temperature distribution for the base flow is such that

$$T_B = \frac{Pe^2}{2}\left(\frac{2}{Bi} + 1 - y^2\right). \tag{44}$$

Nothing changes in the formulation of the fourth order differential equation for Ψ, which is still given by Eq. (33). On the other hand, as

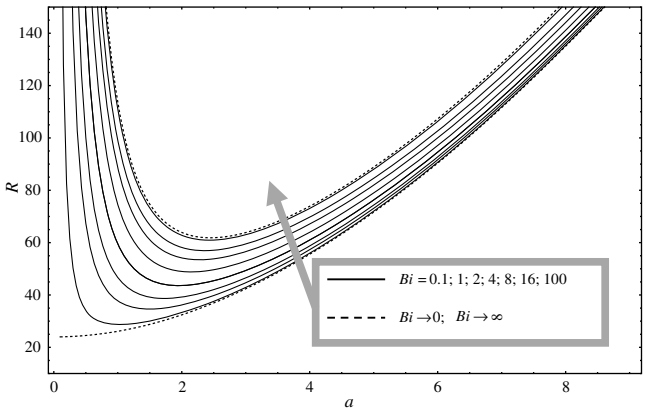

Fig. 7. Neutral stability curves in the (a, R)-plane for different values of Bi.

a consequence of Eqs. (30) and (43), the $y = 1$ boundary condition Eq. (34) is replaced by

$$y = 1: \qquad \Psi = \Psi''' + Bi\,\Psi'' - a^2\,\Psi' = 0. \tag{45}$$

From a mathematical viewpoint, this means that the only practical change in the series solution algorithm is in the definition of the constraint equations at $y = 1$ to determine coefficient A_2, the overall procedure being the same. In the small-G limit, or, equivalently for longitudinal rolls, the effect of different values of Bi on the neutral curve is given in Fig. 7. A perfectly conducting upper boundary corresponds to the limit $Bi \to \infty$, and we see that the

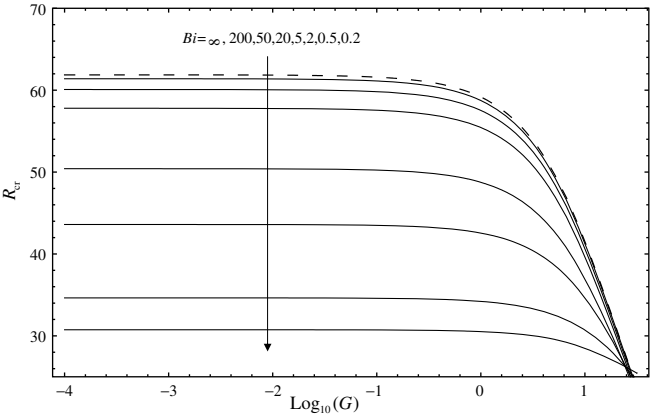

Fig. 8. R_{cr} vs G diagram: plots corresponding to different Bi, the dashed line corresponds to $Bi \to \infty$.

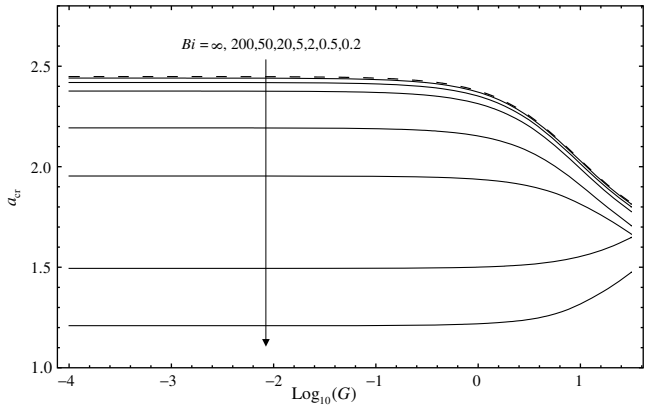

Fig. 9. a_{cr} vs G diagram: plots corresponding to different Bi, the dashed line corresponds to $Bi \to \infty$.

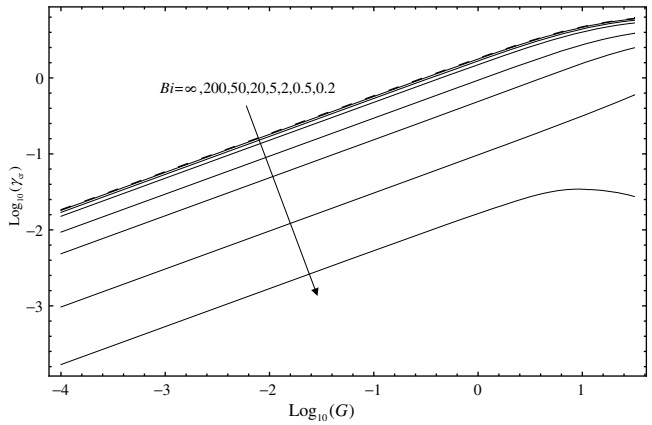

Fig. 10. γ_{cr} vs G diagram: plots corresponding to different Bi, the dashed line corresponds to $Bi \to \infty$.

critical values of both R and a reduce as Bi decreases. In the insulating limit, $Bi \to 0$, we obtain $a_{cr} = 0$, which is consistent with the similar case for the Darcy–Bénard problem; see pp. 193 and 194 of Nield and Bejan [1].

When G takes nonzero values the variation of R_{cr}, a_{cr} and γ_{cr} may be seen in Figs. 8–10, respectively. The variation of R_{cr} with G is given in Fig. 8 where substantial changes in the $G \ll 1$ values occur only as $G \to 1$, an unphysically large value. We see also that R_{cr} reduces as Bi decreases. The corresponding wavenumber variation is shown in Fig. 9. When G takes physically significant values the reduction in the critical wavenumber is monotonic as Bi decreases. Similar behaviour arises for the reduced wavespeed, γ, shown in Fig. 10.

4. Conclusions

In this paper, we have considered horizontal flow in a porous layer where viscous dissipation serves to raise the temperature of the moving fluid. Given that the upper surface of the layer is relatively cold, this means that the thermal profile is potentially thermoconvectively unstable. Our aim has been to determine criteria for the onset of convection. We have found that the parameter R, which plays the role of a Rayleigh number, remains of $O(1)$ magnitude over all physically realistic values of the Gebhart number. From this, it has been possible to determine the critical Péclet number (and the associated wavenumber and phase speed) as a function of the Gebhart number. In general, the transverse roll requires a smaller Péclet number before it is destabilised than any other roll orientation. Other orientations have physical significance when the layer is restricted laterally, and our results may also be applied to these cases. The Appendix gives a large-Péclet asymptotic analysis which gives extremely accurate correlations for all physically realistic values of the Gebhart number.

Appendix A. Asymptotic analysis of rolls as $P \to \infty$

Eqs. (30) and (31) are

$$\Psi'' - a^2\,\Psi + ia\,R\,\Theta = 0, \tag{A1}$$

$$\Theta'' - (i\gamma + a^2)\,\Theta + 2\,P^{-1}\Psi' - ia\,y\,\Psi = 0, \tag{A2}$$

The aim of this Appendix A is to provide an asymptotic analysis of the solutions of the above equations which are valid in the limit of small Ge, or, equivalently, large P. We shall employ the following substitutions,

$$\Psi \to i\,\Psi, \qquad \epsilon = P^{-1}, \tag{A3}$$

to transform Eqs. (A1) and (A2) into a form which is more convenient for the asymptotic analysis. We obtain the system,

$$\Psi'' - a^2\Psi + aR\Theta = 0, \tag{A4}$$

$$\Theta'' - (i\gamma + a^2)\Theta + (2i\Psi')\epsilon + ay\Psi = 0. \tag{A5}$$

According to the numerical results presented earlier, R remains of $O(1)$ throughout the whole physically admissible range of values of Ge. Moreover, the small parameter ϵ, multiplies just one term. In what follows various streamfunction and temperature terms will be defined as part of the asymptotic analysis, and they will all satisfy the boundary conditions given in Eq. (27).

Guided by the numerical results and by the form of the Eqs. (A4) and (A5), we shall introduce the small-ϵ expansions,

$$\Psi = \Psi_0 + \epsilon\Psi_1 + \epsilon^2\Psi_2 + \epsilon^3\Psi_3 + \epsilon^4\Psi_4 + \cdots, \tag{A6}$$

$$\Theta = \Theta_0 + \epsilon\Theta_1 + \epsilon^2\Theta_2 + \epsilon^3\Theta_3 + \epsilon^4\Theta_4 + \cdots, \tag{A7}$$

$$R = R_0 + \epsilon^2 R_2 + \epsilon^4 R_4 + \cdots, \tag{A8}$$

$$\gamma = \epsilon\gamma_1 + \epsilon^3\gamma_3 + \cdots, \tag{A9}$$

and

$$a = a_0 + \epsilon^2 a_2 + \epsilon^4 a_4 + \cdots. \tag{A10}$$

At each stage we equate coefficients of like powers of ϵ to obtain equations for the various Ψ_n and Θ_n terms.

At $O(1)$ we obtain the system,

$$\mathscr{L}_1(\Psi_0, \Theta_0) \equiv \Psi_0'' - a_0^2\Psi_0 + a_0 R_0\Theta_0 = 0, \tag{A11}$$

$$\mathscr{L}_2(\Psi_0, \Theta_0) \equiv \Theta_0'' - a_0^2\Theta_0 + a_0 y\Psi_0 = 0. \tag{A12}$$

Here, we have introduced the notation $\mathscr{L}_n$ for later convenience. This homogeneous system may be solved by setting a normalisation condition such as $\Theta_0(0) = 1$, and then R_0 is found as an eigenvalue. Further terms in (A7) will be taken to satisfy the boundary condition $\Theta_n(0) = 0$.

Eqs. (A11) and (A12) are such that R_0 is a function of the wavenumber, a, and it is necessary to minimise R_0 with respect to a. If we define Ψ_m and Θ_m to be the respective a-derivatives of Ψ_0 and Θ_0, then the a-derivative of Eqs. (A11) and (A12) yield the system,

$$\mathscr{L}_1(\Psi_m, \Theta_m) = 2a_0\Psi_0 - R_0\Theta_0, \tag{A13}$$

$$\mathscr{L}_2(\Psi_m, \Theta_m) = 2a_0\Theta_0 - y\Psi_0, \tag{A14}$$

where we have set $dR_0/da = 0$. The solution of this additional system yields the value of a_0 which minimises R_0.

At $O(\epsilon)$ we obtain,

$$\mathscr{L}_1(\Psi_1, \Theta_1) = 0, \tag{A15}$$

$$\mathscr{L}_2(\Psi_1, \Theta_1) = i\gamma_1\Theta_0 - 2i\Psi_0'. \tag{A16}$$

This is an eigenvalue problem for γ_1 and it may be solved using real arithmetic by means of the substitutions, $\Psi_1 = i\Psi_{1a}$, $\Theta_1 = i\Theta_{1a}$.

At $O(\epsilon^2)$ the resulting system is,

$$\mathscr{L}_1(\Psi_2, \Theta_2) = a_2[2a_0\Psi_0 - R_0\Theta_0] + [-a_0 R_2\Theta_0], \tag{A17}$$

$$\mathscr{L}_2(\Psi_2, \Theta_2) = a_2[2a_0\Theta_0 - y\Psi_0] + i[\gamma_1\Theta_1 - 2\Psi_1']. \tag{A18}$$

Given that the terms multiplying a_2 on the right hand sides of (A17) and (A18) are identical to those on the right hand sides of (A13) and (A14), it is possible to write the solution in the form,

$$\Psi_2 = a_2\Psi_m + \Psi_{2a}, \qquad \Theta_2 = a_2\Theta_m + \Theta_{2a}. \tag{A19}$$

The functions Ψ_{2a} and Θ_{2a} satisfy the system,

$$\mathscr{L}_1(\Psi_{2a}, \Theta_{2a}) = [-a_0 R_2\Theta_0], \tag{A20}$$

$$\mathscr{L}_2(\Psi_{2a}, \Theta_{2a}) = i[\gamma_1\Theta_1 - 2\Psi_1']. \tag{A21}$$

We note that Eqs. (A20) and (A21) have real inhomogeneous terms, and that the system is an eigenvalue problem for R_2. On the other hand, the value of a_2 is not determined at this order, but (A19) shows that one component of the overall second order solution is proportional to a_2, which will be determined at $O(\epsilon^4)$.

At $O(\epsilon^3)$ we have,

$$\mathscr{L}_1(\Psi_3, \Theta_3) = a_2[2a_0\Psi_1 - R_0\Theta_1] - a_0 R_2\Theta_1, \tag{A22}$$

$$\mathscr{L}_2(\Psi_3, \Theta_3) = a_2[2a_0\Theta_1 - y\Psi_1] + i[-2\Psi_2' + \gamma_1\Theta_2 + \gamma_3\Theta_0]. \tag{A23}$$

We note that the inhomogeneous terms are purely imaginary, and given that a_2 appears again as a coefficient, we may split the solution of (A22) and (A23) into two components:

$$\begin{pmatrix} \Psi_3 \\ \Theta_3 \\ \gamma_3 \end{pmatrix} = ia_2 \begin{pmatrix} \Psi_{3a} \\ \Theta_{3a} \\ \gamma_{3a} \end{pmatrix} + i \begin{pmatrix} \Psi_{3b} \\ \Theta_{3b} \\ \gamma_{3b} \end{pmatrix}. \tag{A24}$$

Therefore, we need to solve the two systems of equations,

$$\mathscr{L}_1(\Psi_{3a}, \Theta_{3a}) = 2a_0\Psi_{1a} - R_0\Theta_{1a} + \gamma_{3a}\Theta_0, \tag{A25}$$

$$\mathscr{L}_2(\Psi_{3a}, \Theta_{3a}) = 2a_0\Theta_{1a} - y\Psi_{1a} - 2\Psi_m' + \gamma_1\Theta_m, \tag{A26}$$

and

$$\mathscr{L}_1(\Psi_{3b}, \Theta_{3b}) = -a_0 R_2\Theta_{1a}, \tag{A27}$$

$$\mathscr{L}_2(\Psi_{3b}, \Theta_{3b}) = -2\Psi_{2a}' + \gamma_1\Theta_{2a} + \gamma_{3b}\Theta_0. \tag{A28}$$

These are, respectively, eigenvalue problems for γ_{3a} and γ_{3b}.

Finally, at $O(\epsilon^4)$, the equations are

$$\begin{aligned}\mathscr{L}_1(\Psi_4, \Theta_4) = {} & a_4[2a_0\Psi_0 - R_0\Theta_0] + a_2[-R_2\Theta_0 - R_0\Theta_{2a} \\ & + 2a_0\Psi_{2a} - a_0 R_2\Theta_m] + a_2^2[\Psi_0 + 2a_0\Psi_m \\ & - R_0\Theta_m] - a_0 R_2\Theta_{2a} - a_0 R_4\Theta_0,\end{aligned} \tag{A29}$$

$$\begin{aligned}\mathscr{L}_2(\Psi_4, \Theta_4) = {} & a_4[2a_0 - \Psi_0] + a_2[2a_0\Theta_{2a} - y\Psi_{2a} - \gamma_1\Theta_{3a} + 2\Psi_{3a}'] \\ & + a_2^2[\Theta_0 + 2a_0\Theta_m - y\Psi_{2m}] + 2\Psi_{3b}' \\ & - \gamma_1\Theta_{3b} + \gamma_3\Theta_{1a}.\end{aligned} \tag{A30}$$

This more complicated system may be split into four separate systems for ease of computation:

$$\begin{pmatrix} \Psi_4 \\ \Theta_4 \\ R_4 \end{pmatrix} = a_4 \begin{pmatrix} \Psi_m \\ \Theta_m \\ 0 \end{pmatrix} + a_2^2 \begin{pmatrix} \Psi_{4a} \\ \Theta_{4a} \\ R_{4a} \end{pmatrix} + a_2 \begin{pmatrix} \Psi_{4b} \\ \Theta_{4b} \\ R_{4b} \end{pmatrix} + \begin{pmatrix} \Psi_{4c} \\ \Theta_{4c} \\ R_{4c} \end{pmatrix}. \tag{A31}$$

We have already taken account of the fact that the solution corresponding to a_4 is already known. It is now routine to write out the remaining three systems, but these are omitted for the sake of brevity. However, these three systems form eigenvalue problems for R_{4a}, R_{4b} and R_{4c}, respectively.

This latest solution means that, while R_0 and R_2 are computed constants, the value of R_4 is not; we have

$$R_4 = R_{4a}a_2^2 + R_{4b}a_2 + R_{4c}, \tag{A32}$$

which is a quadratic in a_2. Not surprisingly we find that R_{4a} is positive and therefore a value of a_2 may be found which will minimise R_4. It is,

$$a_2 = -\frac{R_{4b}}{2R_{4a}}. \tag{A33}$$

In turn, this value for a_2 means that the solution at $O(\epsilon^3)$ is now known.

Having solved the full 45th order system (where all the eigenvalues are listed) we obtain the following asymptotic expansions,

$$a \sim 2.44826615 - 4.38433187P^{-2}, \quad \text{(A34)}$$

$$R \sim 61.86656690 - 173.51040218P^{-2} + 851.18063938P^{-4}, \quad \text{(A35)}$$

$$\gamma \sim 14.50695111P^{-1} - 24.42147430P^{-3}. \quad \text{(A36)}$$

All the coefficients are correct to the stated number of decimal places; this required a uniform grid of 1600 equally spaced points using a 4th order Runge Kutta code.

References

[1] D.A. Nield, A. Bejan, Convection in Porous Media, third ed., Springer, New York, 2006.
[2] D.A.S. Rees, Stability of Darcy–Bénard convection, in: K. Vafai (Ed.), Handbook of Porous Media, Begell House, 2000, pp. 521–558.
[3] P.A. Tyvand, Onset of Rayleigh–Bénard convection in porous bodies, in: D.B. Ingham, I. Pop (Eds.), Transport Phenomena in Porous Media II, Elsevier, 2002, pp. 82–112.
[4] C.W. Horton, F.T. Rogers Jr., Convection currents in a porous medium, Journal of Applied Physics 16 (1945) 367–370.
[5] E.R. Lapwood, Convection of a fluid in a porous medium, Proceedings of the Cambridge Philosophical Society 44 (1948) 508–521.
[6] M. Prats, The effect of horizontal fluid flow on thermally induced convection currents in porous mediums, Journal of Geophysical Research 71 (1966) 4835–4838.
[7] D.A.S. Rees, The effect of inertia on the onset of mixed convection in a porous layer heated from below, International Communications in Heat and Mass Transfer 24 (1997) 277–283.
[8] A. Delache, M.N. Ouarzazi, M.-C. Néel, Pattern formation of mixed convection in a porous medium confined laterally and heated from below: effect of inertia, Comptes Rendues Mecanique 330 (2002) 885–891.
[9] A. Postelnicu, Effect of inertia on the onset of mixed convection in a porous layer using a thermal nonequilibrium model, Journal of Porous Media 10 (2007) 515–524.
[10] N. Banu, D.A.S. Rees, Onset of Darcy–Bénard convection using a thermal non-equilibrium model, International Journal of Heat and Mass Transfer 45 (2002) 2221–2228.
[11] D.R. Pitts, L.E. Sissom, Theory and Problems of Heat Transfer – Appendix B, second ed., McGraw-Hill, New York, 1998.